land

MDPI

Article

Spatiotemporal Changes and Driving Force Analysis of Land Sensitivity to Desertification in Xinjiang Based on GEE

Yazhou Zhao [1,2], Shengyu Li [1,*], Dazhi Yang [2,3], Jiaqiang Lei [1] and Jinglong Fan [1]

[1] State Key Laboratory of Desert and Oasis Ecology, Xinjiang Institute of Ecology and Geography, Chinese Academy of Sciences, Urumqi 830011, China; zhaoyazhou20@mails.ucas.ac.cn (Y.Z.)
[2] University of Chinese Academy of Sciences, Beijing 100049, China
[3] Key Laboratory of Land Surface Pattern and Simulation, Institute of Geographic Sciences and Natural Resources Research, Chinese Academy of Sciences, Beijing 100101, China
* Correspondence: oasis@ms.xjb.ac.cn

Abstract: Land desertification profoundly affects economic and social development, thus necessitating a collective response. Regional land control planning needs to assess the land sensitivity to desertification across different regions. In this study, we selected 12 factors from soil, vegetation, climate, and terrain aspects to calculate and evaluate Xinjiang's land sensitivity to desertification, from 2001 to 2020, and analyzed its trends and drivers. The results indicated that the region is highly (22.93%) to extremely sensitive (34.63%) to desertification. Of these, deserts, Gobi lands, oasis–desert transitional zones, and the downstream of rivers are highly and extremely sensitive areas. Mountainous areas, oases, and along rivers are non- and mildly sensitive areas. Over the past two decades, most areas have experienced stability (45.07%) and a slight improvement of desertification (26.18%), while the Junggar Basin and Central Taklamakan Desert have seen slight and severe intensification trends, respectively. Climate-related indicators, such as surface temperature and potential evapotranspiration (PET), were identified as the most important drivers of changes in land sensitivity to desertification. Having an integrated water resource allocation and establishing the long-term monitoring of land sensitivity to desertification would have positive implications for desertification control.

Keywords: land sensitivity to desertification; spatiotemporal changes; Geodetector; Google Earth Engine; Xinjiang

Citation: Zhao, Y.; Li, S.; Yang, D.; Lei, J.; Fan, J. Spatiotemporal Changes and Driving Force Analysis of Land Sensitivity to Desertification in Xinjiang Based on GEE. *Land* **2023**, *12*, 849. https://doi.org/10.3390/land12040849

Academic Editor: Luca Salvati

Received: 9 March 2023
Revised: 27 March 2023
Accepted: 4 April 2023
Published: 8 April 2023

1. Instruction

Land degradation leads to adverse consequences, such as the deterioration of habitat quality and loss of biodiversity, which seriously threaten land security and human life [1,2]. The United Nations included combating desertification as an important topic in the 2030 Agenda for Sustainable Development and the United Nations Convention to Combat Desertification Strategic Framework 2018–2030, with the ultimate goal of reversing desertification and achieving zero growth in land degradation [3]. In fact, under the effect of both natural climate change and intensifying human activities, coupled with unsustainable land management practices, the desertification process is special and complex, so combatting it is too [4–7]. It will be difficult to stop the global desertification process [8,9]. Therefore, it is urgent to understand the current desertification situation, analyze the driving factors, predict the evolution of trends, and formulate response strategies for effective desertification control [10].

Desertification monitoring and assessment is an important prerequisite for prevention and control. Remote sensing satellite data, such as Landsat, Spot, Modis, and QuickBird, provide great assistance in monitoring desertification [11–13]. Remote sensing applications for monitoring desertification fall into two main categories. The first type is to directly use the visual interpretation of remote sensing images or computer classification to understand

the status, quantity, and spatial pattern of land desertification, but samples are influenced by human subjective factors, thus limiting the classification accuracy [14,15]. The second category is to construct models to invert the desertification status by selecting several indicators, focusing on spatial and temporal change monitoring [16,17], dynamic process research [18], and driver analysis [19], such as the Integrated Desertification Index, Desertification Degree Index, Environmental Sensitivity Areas Index (ESAI), etc. The Integrated Desertification Index has uncertainties in selecting assessment indicators and determining indicator weights and rank thresholds [20]. Determining weights in the Integrated Desertification Index mainly refers to local research institutions, technical departments, and the relevant literature, and no uniform standard has been reached. Based on spectral feature information, the Desertification Degree Index was subsequently proposed, but the accuracy of desertification inversion needs to be improved [21]. ESAI originated from Mediterranean desertification. Additionally, the Land Use (MEDALUS) model quantifies the magnitude of the land desertification probability in terms of soil, climate, erosion, vegetation, and human activities and management [22,23]. The MEDALUS model is widely used in Italy [24–26], India [27], Central Asia [28], Greece [29], Iran [30], Turkey [31], Northern China [32], and even worldwide [33]. This model scientifically and flexibly integrates many factors driving desertification processes to provide data support for active and effective desertification monitoring.

Driven by a combination of natural factors and human activities, the desertification process is extremely complex; the land sensitivity to desertification has temporal dynamics and spatial heterogeneity. Clarifying the driving role of factors on land sensitivity to desertification and grasping the main contradictions are important prerequisites for developing effective control plans. Studies have been conducted using Geographically Weighted Regression [26], Random Forest [27], Cluster Analysis [32], and Geodetector [34] on the driving role and driving mechanisms of indicators. Land sensitivity to desertification in Italy is mainly driven by vegetation quality and is more important than land management and climate quality [26], which is consistent with Rajbanshi's study indicating the importance, up to 46%, of vegetation drought resistance [27]. Regions located at different latitudes have different soil and water conditions, resulting in different contributions of vegetation, climate, and soil to the desertification process. Soil and climate play the most direct role in land sensitivity to desertification in the arid zone of northwestern China, while vegetation, which dynamically varies over time, is the most active factor leading to dynamic changes in land sensitivity to desertification [34].

The free sharing and rapid updating of multi-source data, such as remote sensing satellite data, reanalysis data, and meteorological data, have facilitated the progress of large-scale ecological assessments and improved the spatial and temporal resolution of assessment results [35,36]. Before the advent of the Google Earth Engine (GEE), the process of downloading and pre-processing data was time consuming. In fact, users can process data online on GEE and directly export the calculated results, which can reduce the workload of pre-processing data and the storage capacity of intermediate data [37–40]. GEE enables long time series and higher resolution ecological remote sensing model analysis, which provides a unique perspective to assess the land sensitivity of desertification. Of course, GEE has been applied to the land sensitivity to desertification assessment of the Blue Nile Basin [41], and this study provides a good example to further explore the potential of GEE.

Currently, Xinjiang is the most severely desertification-affected area in China and is highly prone to more. With the Three Northern Protected Forest Program being implemented, and the Closed Reserve and the National Desert Park [42–44], the trend of land desertification expansion in Xinjiang has slowed down, but combatting desertification is still necessary. So far, there are few studies on the spatial and temporal dynamics of land sensitivity to desertification in Xinjiang, and the results of continuous assessment are lacking, while the driving force analysis is not deep enough, which is not conducive to a comprehensive grasp of Xinjiang's desertification situation.

Therefore, we quantified Xinjiang's land sensitivity of desertification and explored each evaluation indicator's driving role to fill the gaps in the previous studies. This paper aims to answer three main questions:

(1) What are the spatial and temporal distribution characteristics of Xinjiang's land sensitivity to desertification?
(2) What is the trend of land sensitivity to desertification in the last 20 years?
(3) What is the driving effect of the evaluation indicators on land sensitivity to desertification?

2. Study Area and Data Sources

2.1. Study Area

Sand supply is an important condition for desertification [45]. Xinjiang is in Northwest China's arid region, and, with sparse vegetation, deserts account for more than 80% of its total area. In China, it has both the highest concentration and the widest variety of deserts (Figure 1). Due to the complex mountain–basin landscape pattern, the spatial distribution of precipitation greatly varies [46]. Influenced by the topographic and geomorphological pattern of the mountain–basin system, widespread sediments in the basin, and atmospheric circulation, Xinjiang has windy and sandy environmental characteristics that seriously threaten its infrastructure's safe operation and economic effectiveness. Xinjiang now has more than 1500 km of railways, more than 6000 km of expressways, 164,000 km of highways, many photovoltaic power stations and ditches, and other important projects. The overall potential damage of sandstorms is relatively large. The railways in the southwest edge of the Taklimakan Desert, Alashankou, Dabancheng, and Bailifeng areas have been seriously affected, and the sand burial hazards of many national roads in the Tarim Basin have been serious.

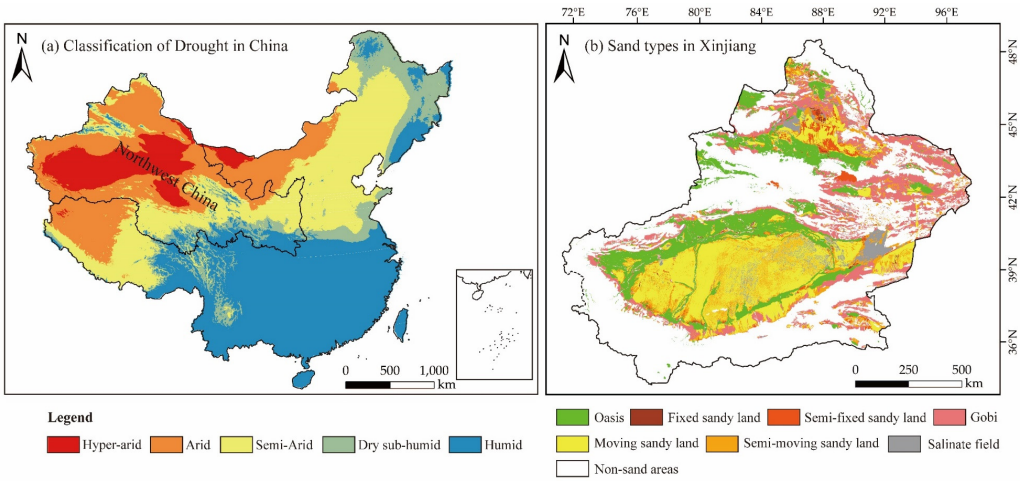

Figure 1. Overview of the study area. (**a**) The classification of drought in China. The degree of drought was classified based on the aridity index, which was divided into hyper-arid (<0.03), arid (0.03–0.2), semi-arid (0.2–0.5), dry sub-humid (0.5–0.65), and humid (>0.65) [47]. (**b**) The sandy types in Xinjiang. Data source: The Aridity index is calculated based on precipitation and evapotranspiration data obtained from TerraClimate [48]. Sand types data were obtained from the National Tibetan Plateau/Third Pole Environment Data Center [49].

2.2. Data Sources

Multiple data were collected (Table 1). The data on soil conditions were obtained from OpenLandMap (https://openlandmap.org, accessed on 9 June 2022), which is a dataset of machine learning predictions based on a global soil profile. The R^2 of soil organic carbon content, sand content, and soil clay content from OpenLandMap, with corresponding sample data, were 83.4%, 90.8%, and 86.0%, respectively. The soil moisture, precipitation, potential evapotranspiration (PET), and average wind speed data were obtained from

TerraClimate, which is a dataset covering the global land surface. The Pearson correlation coefficients of the precipitation and PET from this dataset with the Global Historical Climatology Network and FLUXNET data are 90% and 77%, respectively [50]. MOD13A2 provided the Normalized Difference Vegetation Index (NDVI) data, with a global accuracy of ±0.025 [51]. The vegetation type data were derived from MCD12Q1, which has high applicability in the Chinese region [52]. The surface temperature data were obtained from MOD11A2 with a high spatiotemporal resolution. The NASA Digital Elevation Model provided the Digital Elevation Models (DEM) and slope data. The vertical accuracy RMSE of the China-wide DEM is 8.53 m [53]. To ensure the correctness of the subsequent raster calculations and spatial analysis, the coordinate system for all the raster data was specified to be the WGS84 geographic coordinate system and was resampled to 2.5′. The entire process of this paper using the data and methods is presented in Figure 2.

Table 1. Data sources.

Quality	Indicator	Variable	Spatial Resolution	Data Sources and References	Normalization
Soil	X1	Soil organic carbon content	250 m	OpenLandMap [54]	−
	X2	Soil sand content	250 m	OpenLandMap [55]	+
	X3	Soil clay content	250 m	OpenLandMap [56]	−
	X4	Soil moisture	2.5′	TERRACLIMATE [48]	−
Vegetation	X5	NDVI	1 km	MOD13A2 [57]	−
	X6	Drought resistance	500 m	MCD12Q1 [58]	+
Climate	X7	Precipitation	2.5′	TERRACLIMATE [48]	−
	X8	PET	2.5′	TERRACLIMATE [48]	+
	X9	Surface temperature	1 km	MOD11A2 [59]	+
	X10	Average wind speed	2.5′	TERRACLIMATE [48]	+
Terrain	X11	DEM	30 m	NASADEM [60]	−
	X12	Slope	30 m	NASADEM [60]	−

Notes: the "+" represents the indicator is positively correlated with land sensitivity to desertification, so the indicator is positively normalized. Conversely, "−" is negatively normalized. They were calculated according to Equations (1) and (2).

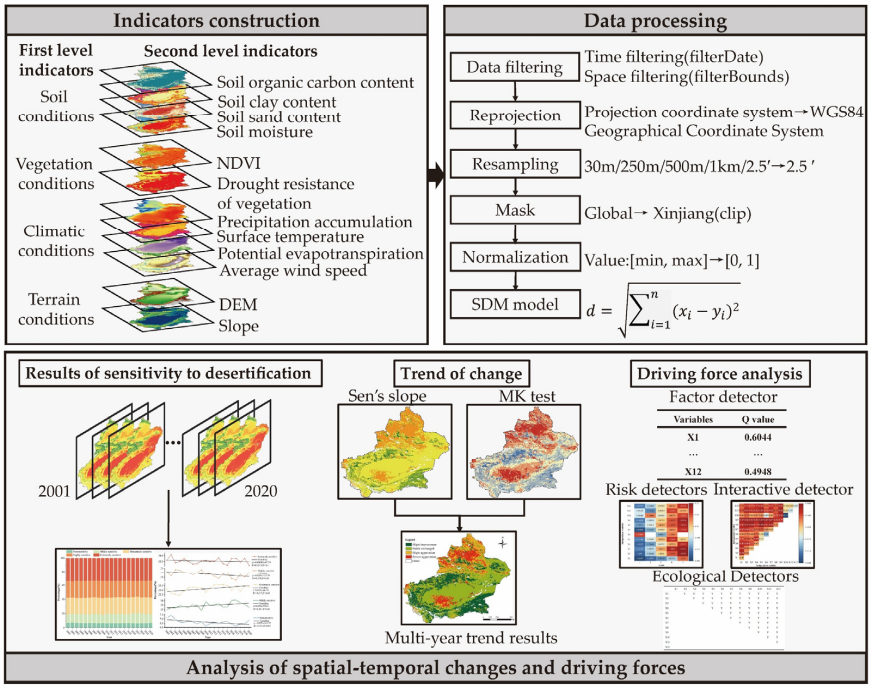

Figure 2. Research framework.

3. Methods

3.1. Assessment of Sensitivity to Desertification

Euclidean distance is widely used in the field of geology [61–63]. In this study, we calculated the desertification sensitivity from the soil, vegetation, climate, and terrain conditions [34]. The raw data were standardized to eliminate the effect of having different indicator scales on desertification sensitivity. The soil organic carbon content, clay content, soil moisture, NDVI, precipitation, DEM, and slope were negatively correlated with the desertification sensitivity and were negatively standardized (Equation (1)). The drought resistance of vegetation, soil sand content, PET, surface temperature, and average wind speed were positively correlated with the desertification sensitivity and were positively standardized (Equation (2)).

$$X_i' = \frac{X_i - \min\{X_i\}}{\max\{X_i\} - \min\{X_i\}} \quad (1)$$

$$X_i' = \frac{\max\{X_i\} - X_i}{\max\{X_i\} - \min\{X_i\}} \quad (2)$$

where X_i is the raster value corresponding to indicator i; $\max\{X_i\}$ is the maximum value of the raster corresponding to that evaluation indicator; $\min\{X_i\}$ is the minimum value of the raster corresponding to that evaluation indicator; and X_i' is the value of indicator i after normalization.

The desertification sensitivity is calculated using the Euclidian distance and the following equation:

$$SI = \sqrt{(SOC - SOC_{low})^2 + (Sand - Sand_{low})^2 + (SC - SC_{low})^2 + (SW - SW_{low})^2} \quad (3)$$

$$VI = \sqrt{(NDVI - NDVI_{low})^2 + (DR - DR_{low})^2} \quad (4)$$

$$CI = \sqrt{(Pre - Pre_{low})^2 + (PET - PET_{low})^2 + (Lst - Lst_{low})^2 + (VS - VS_{low})^2} \quad (5)$$

$$TI = \sqrt{(Dem - Dem_{low})^2 + (Slope - Slope_{low})^2} \quad (6)$$

$$DSI = \sqrt{(SI - SI_{low})^2 + (VI - VI_{low})^2 + (CI - CI_{low})^2 + (TI - TI_{low})^2} \quad (7)$$

where SI is the soil index; SOC is the soil organic carbon content; Sand is the soil sand content; SW is the soil moisture; SC is the soil clay content; VI is the vegetation index; NDVI is the normalized vegetation index; DR is the vegetation drought resistance of vegetation; CI is the climate index; Pre is the precipitation; PET is the potential evapotranspiration; Lst is the surface temperature; VS is the average wind speed; TI is the terrain index; Dem is elevation; and Slope is the slope of the site. The Drought Sensitivity Index (DSI) is the desertification sensitivity, where a higher DSI value indicates a greater likelihood of desertification and vice versa.

3.2. Sen's Slope

Sen's slope is widely used to calculate trends in long-time series data [64,65]. The corresponding formula is as follows:

$$\beta_{DSI} = \text{Median}\left(\frac{DSI_j - DSI_i}{j - i}\right) \forall j > i \quad (8)$$

Where β_{DSI} is the desertification sensitivity trend; DSI_j is the desertification sensitivity raster image element value at time j; and DSI_i is the raster image element value at the time i, corresponding to the position of DSI_j. $\beta_{DSI} > 0$ indicates that the sensitivity to desertification at the corresponding raster image element is increasing during the study period, and $\beta_{DSI} \geq 0.0005$ indicates that the sensitivity to desertification is increasing. When $\beta_{DSI} < 0$, the sensitivity to desertification at the corresponding raster image element is weakened, and when $\beta_{DSI} \leq -0.0005$, the sensitivity to desertification is improved. When $-0.0005 < \beta_{DSI} < 0.0005$, the degree of desertification sensitivity remains largely the same.

3.3. Mann–Kendall Test

The Mann–Kendall test is used to determine whether the trend in the long time series data is significant [66]. We define the Z-statistic as follows:

$$Z = \begin{cases} \frac{S-1}{\sqrt{var(S)}}, S > 0 \\ 0, S = 0 \\ \frac{S+1}{\sqrt{var(S)}}, S < 0 \end{cases} \quad (9)$$

$$S = \sum_{j=1}^{n-1} \sum_{i=j+1}^{n} sgn(DSI_j - DSI_i) \quad (10)$$

$$sgn(DSI_j - DSI_i) = \begin{cases} 1, DSI_j - DSI_i > 0 \\ 0, DSI_j - DSI_i = 0 \\ -1, DSI_j - DSI_i < 0 \end{cases} \quad (11)$$

$$var(S) = \frac{n(n-1)(2n+5)}{20} \quad (12)$$

where n denotes the study time of 20 years and sgn is the sign function. The significance of the changing trend of the desertification sensitivity was judged at the level of significance of $\alpha = 0.05$. When $|Z| > 1.96$, the changing trend of the desertification sensitivity is significant, and the changing trend of the desertification sensitivity is not significant when $|Z| \leq 1.96$.

3.4. Geodetector

The Geodetector method [67] can be used to measure the spatial heterogeneity [68] and has been widely used in desertification [34,69], urbanization [70], landscape [71], and ecological environment quality studies [72].

The factor detector is used to quantitatively reveal the driving force of each evaluation indicator on the desertification sensitivity. The degree that the outcome-independent variable drives the dependent variable has values ranging from 0 to 1.

$$q = 1 - \frac{\sum_{h=1}^{L} N_h \sigma_h^2}{N\sigma^2} = 1 - \frac{SSW}{SST} \quad (13)$$

$$SSW = \sum_{h=1}^{1} N_h \sigma_h^2, \; SST = N\sigma^2 \quad (14)$$

where h = 1, . . . ; L is the stratification of variable Y or factor X; N is the layer h; N_h is the layer h; N is the number of cells in the whole area; σ_h^2 and σ^2 are the variances of the two, respectively; and SSW and SST are the sum of within-stratum variance and the total variance of the whole region, respectively. The larger values of q indicate the greater explanatory power of the independent variable on the dependent variable.

The q-value can measure discretization method's quality and be used as an evaluation criterion for the Geodetector method's results. Different discretization methods yield different q-values [68]. To better reveal the internal driving mechanism of the desertification

sensitivity, we performed an optimal spatial discretization of the independent variables using the multiscale discretization method by comparing the natural breakpoint, the k-mean, and the equidistant interval methods [73]. Obtaining the global optimal discretization using the traditional discretization methods is difficult, while the multi-scale discretization methods can achieve the maximum value of q.

Interaction detectors can be used to identify the interactions between independent variables by comparing the q values of the independent variables X1 and X2 and their interaction (q(X1), q(X2), and q(X1∩X2)). The relationship between two independent variables can be classified as nonlinearly attenuated, one-way nonlinearly attenuated, two-way enhanced, independent, and nonlinearly enhanced.

The risk detector uses the t-statistic to determine whether the difference in the mean values of attributes between two sub-regions are significant.

$$t_{\overline{y}_{h=1}-\overline{y}_{h=2}} = \frac{\overline{Y}_{h=1} - \overline{Y}_{h=2}}{\left[\frac{Var(\overline{Y}_{h=1})}{n_{h=1}} + \frac{Var(\overline{Y}_{h=2})}{n_{h=2}}\right]^{\frac{1}{2}}} \quad (15)$$

where $\overline{Y}_h$ is the mean value of attributes in subregion h; n_h is the number of samples in subregion h; and Var is the variance.

Using ecological detection measures whether the effects of the two independent variables on the dependent variable are significantly different using the F-statistic:

$$F = \frac{N_{X1}(N_{X2} - 1)SSW_{X1}}{N_{X2}(N_{X1} - 1)SSW_{X2}} \quad (16)$$

where N_{X1} and N_{X1} are the sample sizes of the two factors X1 and X2, respectively; SSW_{X1} and SSW_{X1} are the sum of the within-layer variances of the strata formed by X1 and X2; and L1 and L2 denote the number of strata of the variables X1 and X2, respectively.

4. Results

4.1. Spatiotemporal Distribution Patterns of Desertification Sensitivity

The multi-year sensitivity to desertification values in Xinjiang ranges from 0.20–1.52 (Figure 3e). The region is predominantly highly and extremely sensitive to desertification. The desertification sensitivity was classified into five classes using the natural breakpoint method: non-sensitive ($0.2 \leq$ value < 0.64), mildly sensitive ($0.64 \leq$ value < 0.83), moderately sensitive ($0.83 \leq$ value < 0.99), highly sensitive ($0.99 \leq$ value < 1.18), and extremely sensitive ($1.18 \leq$ value ≤ 1.52). The corresponding areas were 104,822, 206,175, 360,743, 362,881, and 548,083 km^2, respectively. Different parts of Xinjiang have different levels of desertification sensitivity (Figure 3f). The Taklamakan Desert, Tuha Basin, Kuruqtag, and Santang-Zhuomao low hills are extremely sensitive areas, where the land cover types are mainly Gobi land and desert. These areas are characterized by abundant sand material, high wind speed, strong evapotranspiration, and scarce precipitation. The Junggar Basin and the northern slope of the east–central part of the Kunlun Mountains are highly sensitive areas. The non-sensitive and mildly sensitive areas are mainly distributed in high-altitude areas with good moisture conditions, far from sand sources, with much precipitation and high vegetation cover.

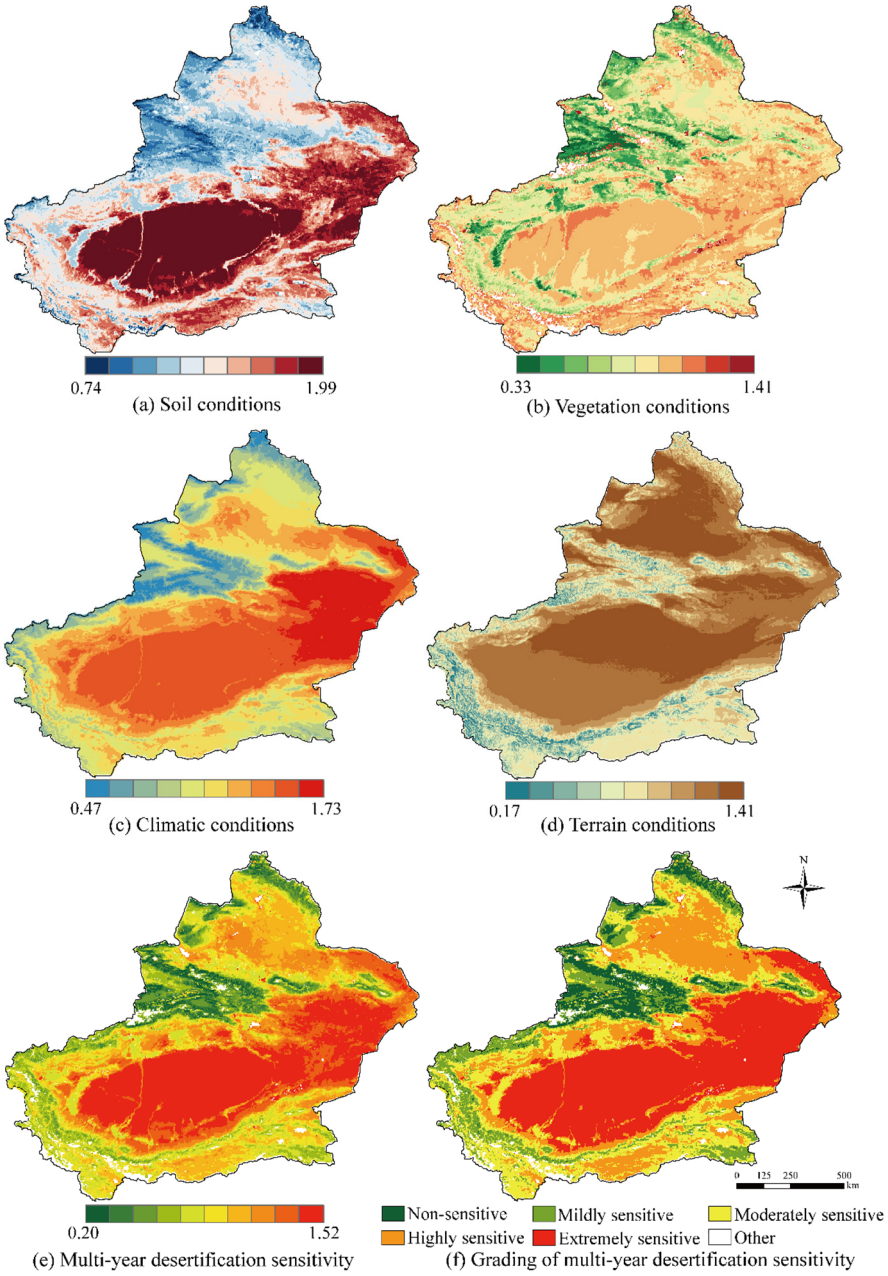

Figure 3. Spatial distribution of first-level indicators, desertification sensitivity, and its classification.

4.2. Spatial Divergence of First-Level Indicators

The vicinities of the Altai, Talhabatai, Tianshan, and Kunlun Mountains and oases are low-value soil condition areas with good soil conditions and low desertification sensitivity. The high-value soil areas with poor soil conditions and high desertification sensitivity are distributed in deserts (Taklamakan Desert, Gurbantunggut Desert, Old Delta Desert of the Peacock River, Kumutag Desert, etc.), Gobi lands (Hashun Gobi, etc.), and saline lands with high soil sand content and low water content, which have soil bases and climatic conditions that are desertification prone.

The high vegetation cover can increase the lower bedding surface's roughness and the starting wind speed value [74]. The vegetation types are horizontally and vertically heterogeneous, and vegetation drought resistance is also spatially heterogeneous. The low-value areas of vegetation conditions (Figure 3b) are distributed near mountains, rivers, and oases with good moisture conditions. The vegetation types are meadows, grasslands,

coniferous forests, alpine vegetation, broadleaf forests, and scrubs, which are the land cover types that have high drought resistance and a low degree of desertification sensitivity.

The climatic conditions (Figure 3c) have obvious spatial heterogeneity due to the influence of the complex topography [75]. The high-value areas are mainly located in the Tuha Basin, Kumtag Desert, Taklamakan Desert, and Gurbantunggut Desert. The highest values of the climatic conditions are distributed in the typical wind areas, such as the western wind area of Turpan, the North Gobi wind area of Hami, the South Gobi wind area of Hami, the Baili wind area, and the Lop Nor wind area. In these areas, the annual number of gale days reaches 50–95 days, and there is strong and frequent potential sand transport with medium–high energy. The resultant drift potential reached 200 VU.

The high-value terrain condition areas (Figure 3d) are mainly located in the desert and Gobi lands at lower elevations and have similarities with the soil, vegetation, and climate conditions. Generally, the areas with high altitudes and steep slopes have relatively better substrate conditions and climatic conditions, which are mainly reflected in the high soil moisture, high vegetation cover, rough substrates, higher precipitation, and, therefore, lower desertification sensitivity.

As can be seen from Table 2, overall, the desertification sensitivity class increases with the increasing soil sand content and PET, and with the decreasing precipitation and soil moisture. As the desertification sensitivity degree increases, the X4 and X7 values show an increasing and then decreasing trend, rather than continuously decreasing. The main reason is that the insensitive areas are in mountainous areas where high elevation and high vegetation cover are dominant factors. The slightly to extremely sensitive areas, on the other hand, respond to soil water and precipitation to a greater extent, and elevation is not the dominant factor.

Table 2. Statistics of evaluation indexes corresponding to each level of desertification sensitivity.

Level	Area (km^2)	X2	X4	X7	X8	X10
Non-sensitive	104,822.3	23–65	0.1–73.85	1.74–55.82	8.13–84.88	1.36–4.72
Mildly sensitive	206,175.1	20–73	0–132.5	1.25–56.34	0.04–96.36	1.15–5.11
Moderately sensitive	360,743	23–85	0–68.3	1.17–54.13	0–118.11	1.09–5.51
Highly sensitive	3,628,81.5	28–93	0–62.8	1.11–52.76	0–132.49	1.08–5.15
Extremely sensitive	548,083.3	30–100	0–22.9	0.93–23.73	1.45–140.55	1.06–5.03

Notes: the X2 independent variable is soil sand content. The X4 independent variable is soil moisture. The X7 independent variable is precipitation. The X8 independent variable is PET. The X10 independent variable is average wind speed.

4.3. Temporal Trends in Desertification Sensitivity

From 2001 to 2020, the percentages of extremely, highly, and non-sensitive areas showed a decreasing trend, while the proportions of mildly and moderately sensitive areas increased. The overall trend of the multi-year desertification sensitivity was mainly stable (45.07%) and slightly improved (26.18%).

The percentages for each desertification sensitivity level from 2001 to 2020 are shown in Figure 4a. The highest percentage is extremely sensitive, while the lowest percentage is insensitive and mildly sensitive. The evolution of the percentages of each desertification sensitivity level (Figure 4b) shows that extreme, high, and insensitivity decreased at the rate of 0.00689/a, 0.055/a, and 0.029/a, respectively. Mild and moderate sensitivity decreased at the rate of 0.056/a and 0.035/a, respectively.

The multi-year trend of the desertification sensitivity in Xinjiang (Figure 5) is mainly characterized by stability and slight improvement. The percentages of the pixels with stability, slight improvement, slight aggravation, and severe aggravation are 45.07%, 26.18%, 16.97%, and 11.78%, respectively. The slight improvements are mainly found in the Kunlun Mountain-Algin Mountain, Tarim River Basin, and Northern Tianshan. Stability is mainly found in the Santang-Zhuomao low hills, Tuha Basin, and Tarim Basin. Slight aggravations are mainly distributed in the Altay Mountain and Tianshan Mountain. Severe aggravations

are found in the Gurbantunggut Desert and South–Central Taklamakan Desert. Overall, the desertification sensitivity in northern Xinjiang tends to increase, while, in southern Xinjiang, it is mainly stable and slightly improved, and the desertification sensitivity tends to decrease.

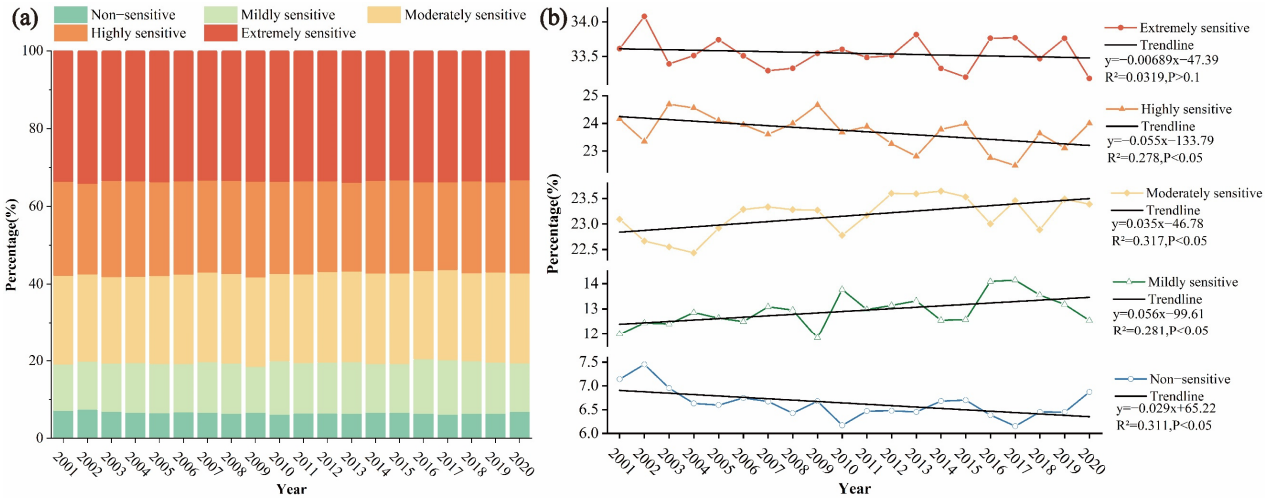

Figure 4. Proportion of image elements of each level of desertification sensitivity and sensitivity trends. (**a**) The percentages for each desertification sensitivity level from 2001 to 2020. (**b**) The evolution of the percentages of each desertification sensitivity level.

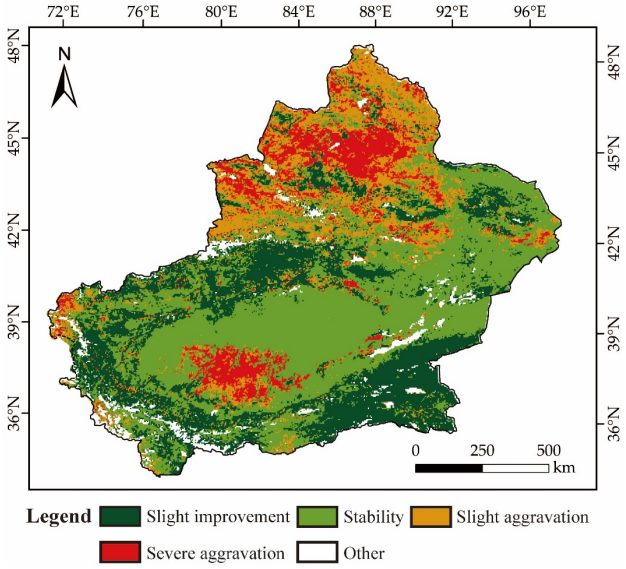

Figure 5. Spatial distribution of multi-year desertification sensitivity trends.

Areas such as Gobi land, the downstream of rivers, and desert–oasis transition zones are sensitive. Desert vegetation acts as wind and sand control, promoting soil and water conservation and water retention [76]. Additionally, vegetation serves as a buffer in the dynamic transition of different levels of sand sensitivity, while precipitation is the most important driver of desert vegetation growth [77,78]. Significant desert vegetation degradation is closely related to long-term drought, and annual precipitation is vital in desert vegetation growth [79]. The multi-year precipitation minimums in Xinjiang (Figure 6) show that the Junggar Basin received the least precipitation from 2014 to the present; the western Tarim Basin received the least precipitation in 2001, 2009, and 2020; the Tuha Basin received the least precipitation in 2006 and 2009; and the Kunlun Mountains-Arjinshan received the least precipitation in 2001 and 2009. Given the spatiotemporal dynamics of

regional precipitation, desert vegetation is in a vulnerable state. Short-lived vegetation in Xinjiang is only distributed in the Junggar Basin and accounts for 37.1% of the total regional desert vegetation. This vegetation relies on snowmelt and precipitation to rapidly complete its growth process within two months [80]. Growing season precipitation is a critical water supply for the desert vegetation [79]. The desertification sensitivity in the Gobi land, desert–oasis transition zones, and downstream of rivers is mildly, moderately, and highly desertification sensitive, and the regional desertification process is easily aggravated by external disturbance. The above areas are key control areas of land desertification. The ecological risk of areas with high sand source abundance is relatively stable, and the human disturbance should be minimized to protect the natural environment.

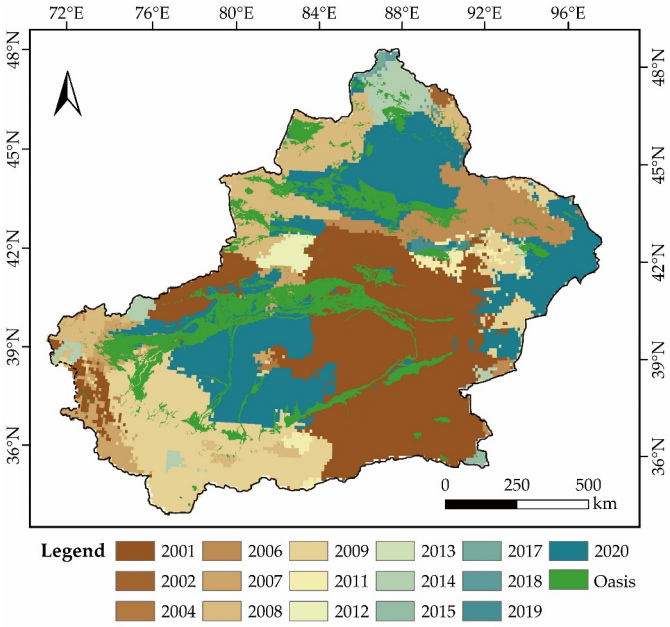

Figure 6. Years corresponding to the minimum annual precipitation in Xinjiang from 2001 to 2020.

4.4. Attribution Analysis of Desertification Sensitivity

To reduce the data storage capacity and significantly improve the code's running speed, the continuous-type independent and dependent variables were multiplied by 1000 and rounded to integer raster data before applying the multiscale discretization method. Using the multiscale discretization method, the nodes of the independent variable X were obtained and reclassified (Table 3).

Table 3. Nodes, q-values, and significance of the independent variable X.

Variable	Nodes				q Value	Sig
X1	1000	2000	3000	5000	0.6044	0.000 *
X2	20,000	60,000	71,000	87,000	0.6570	0.000 *
X3	1000	6000	12,000	22,000	0.6025	0.000 *
X4	213	513	3706	6080	0.6477	0.000 *
X5	302,267	625,165	833,485	1,431,314	0.5457	0.000 *
X7	3537	7112	15,150	22,995	0.6153	0.000 *
X8	74,234	89,028	93,355	101,084	0.6668	0.000 *
X9	286,382	292,918	297,981	301,940	0.7946	0.000 *
X10	1640	2002	3078	3428	0.1676	0.000 *
X11	7870	14,030	19,090	38,590	0.4706	0.000 *
X12	136	1166	2050	3728	0.4948	0.000 *
X6	—	—	—	—	0.3776	0.000 *

Notes: The "*" represents the sig values were all less than 0.01 and passed the significance test. "X6" is a discrete variable, so there is no node and it is marked with "—".

In descending order, the q-values were as follows: surface temperature > PET > soil sand content > soil moisture > precipitation > soil organic carbon content > soil clay content > NDVI > slope > elevation > drought resistance of vegetation > wind speed (Table 3). The desertification sensitivity in Xinjiang is mainly determined by its climate and soil. Climate conditions are the most important conditions affecting desertification sensitivity, followed by soil conditions, while vegetation and terrain conditions have weaker explanatory power for the desertification sensitivity. Among the climatic conditions, the two most significant elements influencing the desertification sensitivity are the surface temperature and PET, with explanatory powers of 79.46% and 66.68%, respectively. Among the soil conditions, the explanatory powers of the soil sand content, soil moisture, soil organic carbon content, and soil clay content on desertification sensitivity are 65.7%, 64.77%, 60.44%, and 60.25%, respectively.

The interannual desertification sensitivity trends (Figure 5) show that the desertification of the Junggar Basin and the Central Taklamakan Desert are being slightly and severely intensified, respectively. There is a strong correlation between the surface temperature and PET in determining the desertification sensitivity. The Sen's slope analysis of both areas (Figure 7) shows that there are large intensification trends in both the Junggar Basin and Taklamakan Desert, which is consistent with the spatial distribution of the desertification sensitivity trends. To quantify the relationship between the changing desertification sensitivity trend and the surface temperature and PET, 1000 points were randomly selected, and a correlation analysis was performed. The change trend values of the surface temperature and PET were positively correlated with the desertification sensitivity change trend values, with correlation coefficients of 0.3194 and 0.3498, respectively. This indicates that changes in the surface temperature and PET are important factors leading to changes in desertification, which confirms the conclusions from using Geodetector analysis [81–83].

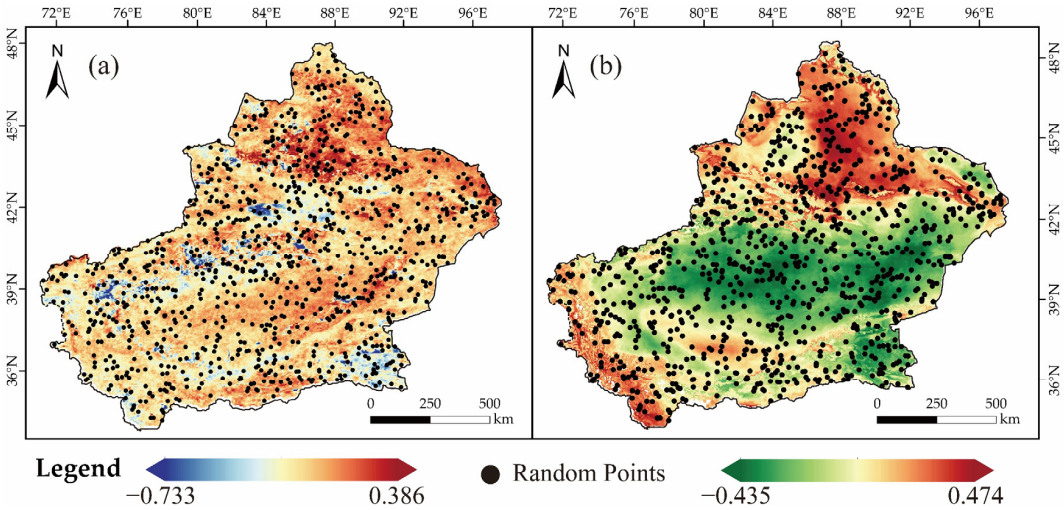

Figure 7. (**a**) The Sen's slope of surface temperature. (**b**) The Sen's slope of PET. A Sen's slope value less than 0 indicates an increasing trend. On the contrary, there is a decreasing trend [64,65].

Figure 8 showed that the different independent variable levels correspond to the mean desertification sensitivity values. The slope is one of the factors that reflects the terrain's complexity and indirectly affects the desertification sensitivity by influencing the slope's soil erosion degree [84]. The regional topographic relief gradually increases with the slope, which increases the soil stability and has an inhibitory effect on the desertification process. Wind speed is the dynamic condition that generates wind and sand displacement and determines the resultant drift potential. Overall, the mean value of the desertification sensitivity increases with the mean wind speed class. The surface temperature was found to positively relate to the PET and negatively relate to the precipitation. The mean desertification sensitivity values of the surface temperature, PET, and precipitation increased

at rates of 0.1356 (R^2 = 0.9976), 0.1188 (R^2 = 0.9915), and 0.1455 (R^2 = 0.9913), respectively. The desertification sensitivity values did not increase with the drought resistance of vegetation, and the mean values of the desertification sensitivity corresponding to the drought resistance of levels 1, 3, and 4 were 1.18, 0.80, and 1.12, respectively. Some areas with level 1 vegetation drought resistance have low desertification sensitivity. The areas with level 3 and 4 drought resistance have high ecological sensitivity and the land is prone to sand encroachment. However, through implementing key sand control projects, such as closure and protection, non-irrigated afforestation, and the return of cultivated land to forests, sandy land area expansion has been slowed down; thus, human intervention has reduced the region's desertification sensitivity. The soil clay content, soil sand content, and soil organic carbon content directly reflect the sand material richness of the sub-bedding surface, and the desertification sensitivity value increases with the sand material richness.

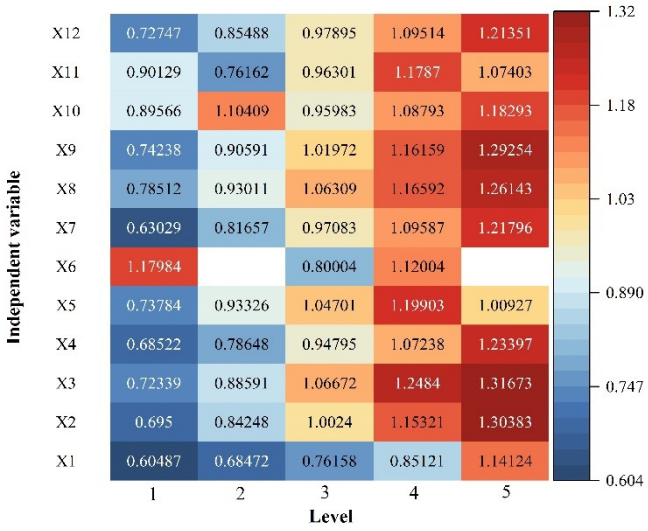

Figure 8. Risk detector results.

The interaction detector results in Figure 9 show that the interaction of any two independent variables contributes more to the desertification sensitivity than a single independent variable, and that the desertification sensitivity is the result of complex interactions among the factors. Figure 10 shows that the effects of the soil clay and soil organic carbon contents on the desertification sensitivity spatial distribution were not significant, and that the spatial distributions of both were similar. However, the effects of any two remaining factors on the spatial distribution of the desertification sensitivity were significant.

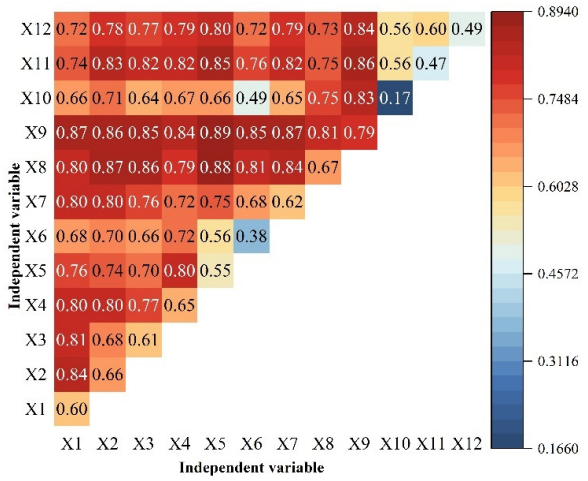

Figure 9. Interaction detector results.

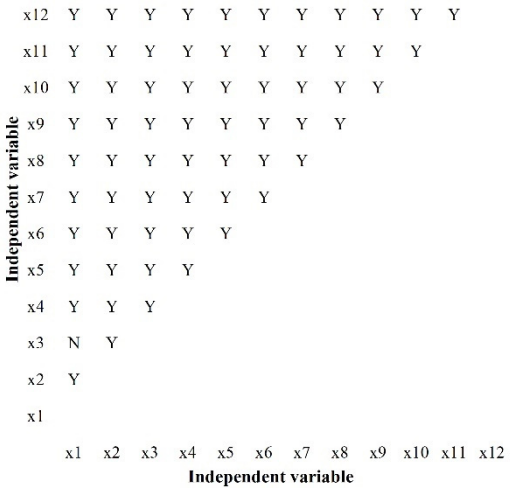

Figure 10. Ecological detection results. Notes: "Y" indicates that there is a significant difference between the two independent variables on desertification sensitivity. "N" indicates that there is no significant difference between the two independent variables on desertification sensitivity.

5. Discussion

5.1. Evaluation Indicators Selection

The MEDALUS model shows great flexibility, reliability and comprehensiveness in indicator selection and framework construction, a variety of data sources, adaptability to a wide range of spatial scales, and the ability to select indicators and flexibly choose weights according to the study area's conditions. It selects indicators in terms of soil, climate, vegetation, management, and human activities [27,28,31,41,85]. Regarding the soil quality, common indicators include parent material, rock fragments, soil depth, soil gradient, soil structural decline, salinization, electrical conductivity, topsoil clay composition, drainage, soil erosion, etc. Regarding the climate quality, common indicators include precipitation, aridity, aspect, wind erosion index, wind speed, etc. Regarding the vegetation quality, common indicators include fire risk, soil erosion protection, plant drought resistance, plant cover, etc. Regarding the management and human activity quality, common indicators include population density, annual growth, grazing pressure, land use, policy implementation, agricultural intensity, etc. Even Karavitis et al. [86] selected 98 indicators to construct a desertification risk index in terms of the soil erosion, cropland erosion, soil salinization, water stress, overgrazing, and wildfires. This confirms the MEDALUS model's flexibility in indicator selection, but it raises two questions: is it necessary to select so many indicators? How do you determine the indicator system? In fact, multicollinearity among indicators is inevitable [87], and the accuracy and value of land sensitivity to desertification obtained by referring to traditional indicator systems, without trade-offs, is indeed questionable. Of course, the Geodetector method used in this study accounts for the multicollinearity problem [68].

Therefore, in the existing land sensitivity to desertification evaluation in China, the indicator system's construction fully accounts for the actual local conditions, which provides a sufficient reference for determining the study's indicators. Assessing the land sensitivity to desertification in China began with assessing ecological sensitivity [88]. The index system of the land sensitivity to desertification evaluation in the Qinghai Lake Basin includes the wetness index, windy days, soil texture, and vegetation cover [89]. The index system of desertification sensitivity evaluation in Inner Mongolia includes dryness, number of windy days in winter and spring, proportion of sandy land, soil texture, rate of change in forest and grassland, and NDVI [90]. Xu et al. [85] studied the land sensitivity to desertification in northern China from 1981 to 2010 and projected future scenario changes from 2011 to 2030. We note that the land management quality index contains grazing pressure and population pressure data, which are derived from the statistical yearbook

of the northern provinces, but the statistical yearbook data can only provide results for administrative units, not continuous data, and cannot fully reflect land management's spatial heterogeneity. In summary, the simple construction of the indicator system of the land sensitivity to desertification study in the Chinese region, which is less complicated than the traditional MEDALUS model, has also achieved good results, which indicates that the evaluation indicator system's construction is of key significance for desertification sensitivity assessment.

In this study, Xinjiang's natural climate and topography were fully considered when developing the index system; thus, the soil quality, vegetation quality, climate quality, and terrain quality were selected, and land management was not. The two indicators of the grazing pressure and population pressure, which are commonly used in land management quality, are not applicable in Xinjiang. On the one hand, the pastoral areas in Xinjiang, concentrated in the Tianshan Mountains, with high altitudes and numerous nature reserves, have been established, meaning the desertification risk in the pastoral areas is minimal [91,92]. On the other hand, only using the population density to quantify the population pressure is not convincing for corroborating that urbanization has a catalytic effect on the desertification process. In addition, the data source of these two indicators is also a problem, and we believe that the statistical yearbook provides the results of the administrative divisions without spatial continuity, which weakens the accuracy of the land sensitivity to desertification. The land management quality index only shows high values in the western Tarim Basin, while the land management quality index is low in the Tarim River Basin, the Tuha Basin, and the Junggar Basin. However, according to the authors' fieldwork in Xinjiang, human activities threatening the oasis have intensified the desertification process that should be regarded as high, but, unfortunately, the land management quality index results have a large gap with reality, so the land management quality may increase the error of land sensitivity to the desertification assessment results [85]. Therefore, considering the water and soil conditions in Xinjiang, we selected 12 indicators related to land sensitivity to desertification, without considering the land management quality.

5.2. Comparison with Previous Studies

Our study suggests that Xinjiang's spatial distribution of land sensitivity to desertification is characterized by low values in its mountainous areas and high values in its basins. This is consistent with many studies, although there are some differences in the fine details, subject to different data sources and assessment models. Xu et al. highlights that the Tarim Basin is an area of high desertification sensitivity, and the increase in rainfall and decrease in aridity are important reasons for the decreasing desertification sensitivity trend in the eastern Tarim Basin, while the increasing population pressure leads to the increasing desertification sensitivity trend in the Hami-Turpan Basin [85]. Since 2001, the Tarim River Basin Authority has constructed major projects, such as irrigation district water conservation, plain reservoir renovation, groundwater development and utilization, river training, the Bosten Lake water transfer project, ecological construction, the mountain reservoir control project, basin water resources scheduling and management, etc. A total of 485 individual projects have been completed and put into operation. The ecological management of the Tarim River Basin has achieved significant results [42,93]. Therefore, it is debatable that the land sensitivity to desertification in the western part of the Tarim Basin is increasing. It further confirms that it is reasonable not to choose land management quality in this study. The conversion characteristics of the desertification sensitivity in the arid zone of Northwest China were obtained based on the spatial overlay of the desertification sensitivity levels in 2000, 2005, 2010, and 2017, and, thus, a lot of the information was inevitably lost [34]. Additionally, this paper analyzes the desertification sensitivity values from 2001 to 2020, using an MK test and Sen's slope, to more carefully reveal the change trend of land sensitivity to desertification.

When analyzing the drivers of desertification sensitivity, many studies in the Chinese region have pointed out that climate is the driving condition for the desertification process

and soil is the material basis for desert formation. The increase in regional rainfall, decrease in windy days, and establishment of ecological projects, such as the project of returning farmland to forest, the project of returning pasture to grass, and the project of sanding control, have effectively reduced the land sensitivity to desertification [34,88,94]. In conclusion, we integrated the existing studies and fully integrated the study area's situation, selected the evaluation index system, obtained the scientific desertification sensitivity assessment results and change trends, and quantitatively revealed the driving effect of the indicators on land sensitivity to desertification.

5.3. Policy Implication

With a soaring population, water resource overexploitation, and the overuse of land natural resources, the desertification sensitivity of desert–oasis transition zones and the downstream of rivers is unstable. Direct human intervention in land use has led to an uneven distribution of water resources, which has resulted in the simultaneous expansion of oases and deserts. The desert oasis transition zones have an extremely important role in suppressing desertification's forward movement and are showing a trend of narrowing. Therefore, in the future, for the integrated ecological management of basins, water resources must be uniformly allocated from the perspective of the whole basin [42].

Constructing a reasonable index system, comprehensively determining the weights of evaluation indexes, and establishing a scientific monitoring platform for desertification sensitivity can provide an early warning mechanism for desertification control. Incorporating data from future climate change scenarios into assessment models, such as those provided by the Coupled Model Intercomparison Project, can aid in building more scientific desertification sensitivity assessment models and projection results. Using the desertification sensitivity assessment results as a reference, we should focus on improving the dominant drivers, pay attention to the areas where desertification is expected to increase in the future, and, accordingly, carry out sand prevention and control measures. In northern Xinjiang, protecting natural vegetation and installing engineering measures for protection are the main focus. In southern Xinjiang, the vast area of mobile deserts, sparse vegetation, and severe scarcity of water resources cause it to be extremely important to carry out targeted protective forest management, river tailrace restoration, and infrastructure protection against wind and sand hazards.

6. Conclusions

We evaluated Xinjiang's desertification sensitivity from 2001 to 2020 based on GEE and analyzed its spatiotemporal change patterns and driving forces, with the following main conclusions:

Areas in Xinjiang are mainly highly (36.29×10^4 km^2) and extremely sensitive to desertification (54.81×10^4 km^2). The desert areas are mainly highly and extremely sensitive. Human disturbance should be minimized to protect these ecosystems. The mildly, moderately, and highly sensitive areas are distributed in the sensitive and fragile areas, such as mountains, Gobi land, desert–oasis transition zones, and the downstream of rivers; these are areas that are easily disturbed by human activities and climate change and are key prevention and control areas.

The change rate of each desertification sensitivity grade is slow. The percentages of extremely (0.00689/a), highly (0.055/a), and non-sensitive land (0.029/a) are decreasing, and the percentages of mildly (0.056/a) and moderately sensitive land (0.035/a) are increasing. The multi-year trend of desertification sensitivity in Xinjiang is dominated by slight improvement and stability, among which the percentages of slight improvement, stability, slight aggravation, and severe aggravation are 26.18%, 45.07%, 16.97%, and 11.78%, respectively. Long-term climate change caused a slight improvement and severe intensification of the desertification sensitivity in the Junggar Basin and central Taklamakan Desert.

The Geodetector study's results showed that the desertification sensitivity in Xinjiang is mainly driven by climate and soil conditions, followed by vegetation and terrain condi-

tions, and that the explanatory powers of the surface temperature and PET are 79.46% and 66.68%, respectively.

Sand control and management in Xinjiang must be based on scientific knowledge of sandy land, understanding the formation and evolution of the windy and sandy environment, the spatial distribution pattern, and careful consideration of sandy land characteristics. Based on scientific facts, sensitive areas of sandy land in Xinjiang are mainly located on the edges of the oasis, downstream of rivers, and tailing lakes, which are the critical areas for sand control in Xinjiang. Alternatively, we need to scientifically quantify the regional wind and sandy hazard laws to improve the monitoring model and early warning system for sandy land. On the other hand, according to the scientifically coordinated allocation of water resources, we should improve the efficiency of water use and promote the research, development, and application of new technologies, materials, and methods to achieve sustainable operations and management.

Author Contributions: Conceptualization, S.L. and J.L.; formal analysis, Y.Z., D.Y. and S.L.; investigation, Y.Z. and S.L.; resources, J.F.; writing—original draft preparation, Y.Z., D.Y. and S.L.; writing—review and editing, Y.Z. and S.L.; supervision, S.L. All authors have read and agreed to the published version of the manuscript.

Funding: This research was funded by the Third Xinjiang Scientific Expedition Program (Grant No. 2021xjkk0305) and Key R&D projects of the National Forestry and Grassland Administration in 2021 (Grant No GLM [2021] 100).

Data Availability Statement: The data presented in this study are available in figures and tables provided in the manuscript.

Acknowledgments: We thank the editor and anonymous reviewers for their useful feedback that improved this paper.

Conflicts of Interest: The authors declare no conflict of interest.

References

1. Wang, Y.; Zhang, J.; Tong, S.; Guo, E. Monitoring the trends of aeolian desertified lands based on time-series remote sensing data in the Horqin Sandy Land, China. *Catena* **2017**, *157*, 286–298. [CrossRef]
2. Sarparast, M.; Ownegh, M.; Sepehr, A. Evaluating the impacts of combating-action programs on desertification hazard trends: A case study of Taybad-Bakharz region, northeastern Iran. *Environ. Sustain. Indic.* **2020**, *7*, 100043. [CrossRef]
3. Chasek, P.S. The convention to combat desertification: Lessons learned for sustainable development. *J. Environ. Dev.* **1997**, *6*, 147–169. [CrossRef]
4. Hulme, M.; Kelly, M. Exploring the links between desertification and climate change. *Environ. Sci. Policy Sustain. Dev.* **1993**, *35*, 4–45. [CrossRef]
5. Sivakumar, M.V.K. Interactions between climate and desertification. *Agric. For. Meteorol.* **2007**, *142*, 143–155. [CrossRef]
6. Alibekov, L.; Alibekov, D. Causes and Socio-Economic Consequences of Desertification in Central Asia: Causes and Consequences of Desertification. In *The Socio-Economic Causes and Consequences of Desertification in Central Asia*; Springer: Berlin/Heidelberg, Germany, 2008. [CrossRef]
7. Feng, Q.; Tian, Y.; Yu, T.; Yin, Z.; Cao, S. Combating desertification through economic development in northwestern China. *Land Degrad. Dev.* **2019**, *30*, 910–917. [CrossRef]
8. Mabbutt, J.A. A new global assessment of the status and trends of desertification. *Environ. Conserv.* **1984**, *11*, 103–113. [CrossRef]
9. Ma, X.; Zhu, J.; Yan, W.; Zhao, C. Projections of desertification trends in Central Asia under global warming scenarios. *Sci. Total Environ.* **2021**, *781*, 146777. [CrossRef]
10. Stringer, L.C.; Dyer, J.C.; Reed, M.S.; Dougill, A.J.; Twyman, C.; Mkwambisi, D. Adaptations to climate change, drought and desertification: Local insights to enhance policy in southern Africa. *Environ. Sci. Policy* **2009**, *12*, 748–765. [CrossRef]
11. Ma, Z.; Xie, Y.; Jiao, J.; Wang, X. The construction and application of an Aledo-NDVI based desertification monitoring model. *Procedia Environ. Sci.* **2011**, *10*, 2029–2035. [CrossRef]
12. Lamchin, M.; Lee, J.-Y.; Lee, W.-K.; Lee, E.J.; Kim, M.; Lim, C.-H.; Choi, H.-A.; Kim, S.-R. Assessment of land cover change and desertification using remote sensing technology in a local region of Mongolia. *Adv. Space Res.* **2016**, *57*, 64–77. [CrossRef]
13. Zerrouki, Y.; Harrou, F.; Zerrouki, N.; Dairi, A.; Sun, Y. Desertification detection using an improved variational autoencoder-based approach through ETM-landsat satellite data. *IEEE J. Sel. Top. Appl. Earth Obs. Remote Sens.* **2020**, *14*, 202–213. [CrossRef]
14. Tripathy, G.; Ghosh, T.; Shah, S. Monitoring of desertification process in Karnataka state of India using multi-temporal remote sensing and ancillary information using GIS. *Int. J. Remote Sens.* **1996**, *17*, 2243–2257. [CrossRef]

15. Afrasinei, G.-M.; Melis, M.T.; Buttau, C.; Arras, C.; Pistis, M.; Zerrim, A.; Guied, M.; Ouessar, M.; Essifi, B.; Zaied, M.B. Classification methods for detecting and evaluating changes in desertification-related features in arid and semiarid environments. *Euro-Mediterr. J. Environ. Integr.* **2017**, *2*, 1–19. [CrossRef]
16. Tomasella, J.; Vieira, R.M.S.P.; Barbosa, A.A.; Rodriguez, D.A.; de Oliveira Santana, M.; Sestini, M.F. Desertification trends in the Northeast of Brazil over the period 2000–2016. *Int. J. Appl. Earth Obs. Geoinf.* **2018**, *73*, 197–206. [CrossRef]
17. Zhang, J.; Guan, Q.; Du, Q.; Ni, F.; Mi, J.; Luo, H.; Shao, W. Spatial and temporal dynamics of desertification and its driving mechanism in Hexi region. *Land Degrad. Dev.* **2022**, *33*, 3539–3556. [CrossRef]
18. Hillel, D.; Rosenzweig, C. Desertification in relation to climate variability and change. *Adv. Agron.* **2002**, *77*, 1–38. [CrossRef]
19. Guo, B.; Wei, C.; Yu, Y.; Liu, Y.; Li, J.; Meng, C.; Cai, Y. The dominant influencing factors of desertification changes in the source region of Yellow River: Climate change or human activity? *Sci. Total Environ.* **2022**, *813*, 152512. [CrossRef]
20. Santini, M.; Caccamo, G.; Laurenti, A.; Noce, S.; Valentini, R. A multi-component GIS framework for desertification risk assessment by an integrated index. *Appl. Geogr.* **2010**, *30*, 394–415. [CrossRef]
21. Lamqadem, A.A.; Saber, H.; Pradhan, B. Quantitative assessment of desertification in an arid oasis using remote sensing data and spectral index techniques. *Remote Sens.* **2018**, *10*, 1862. [CrossRef]
22. Kosmas, C.; Kirkby, M.; Geeson, N. *The MEDALUS Project: Mediterranean Desertification and Land Use*; Manual on key indicators of Desertification mapping environmental sensitive areas to desertification; European Commission: Office for Official Publications of the European Communities: Luxembourg, 1999.
23. Sterk, G.; Boardman, J.; Verdoodt, A. Desertification: History, causes and options for its control. *Land Degrad. Dev.* **2016**, *27*, 1783–1787. [CrossRef]
24. Salvati, L.; Bajocco, S. Land sensitivity to desertification across Italy: Past, present, and future. *Appl. Geogr.* **2011**, *31*, 223–231. [CrossRef]
25. Salvati, L.; Zitti, M.; Perini, L. Fifty years on: Long-term patterns of land sensitivity to desertification in Italy. *Land Degrad. Dev.* **2016**, *27*, 97–107. [CrossRef]
26. Egidi, G.; Cividino, S.; Paris, E.; Palma, A.; Salvati, L.; Cudlin, P. Assessing the impact of multiple drivers of land sensitivity to desertification in a Mediterranean country. *Environ. Impact Assess. Rev.* **2021**, *89*, 106594. [CrossRef]
27. Joy, R.; Das, S. Monitoring land sensitivity to desertification using the ESAI approach and evaluation of the key indicators: A spatio-temporal study in India. *Land Degrad. Dev.* **2021**, *32*, 3045–3061. [CrossRef]
28. Jiang, L.; Bao, A.; Jiapaer, G.; Guo, H.; Zheng, G.; Gafforov, K.; Kurban, A.; De Maeyer, P. Monitoring land sensitivity to desertification in Central Asia: Convergence or divergence? *Sci. Total Environ.* **2019**, *658*, 669–683. [CrossRef]
29. Kairis, O.; Karamanos, A.; Voloudakis, D.; Kapsomenakis, J.; Aratzioglou, C.; Zerefos, C.; Kosmas, C. Identifying degraded and sensitive to desertification agricultural soils in Thessaly, Greece, under simulated future climate scenarios. *Land* **2022**, *11*, 395. [CrossRef]
30. Sepehr, A.; Hassanli, A.; Ekhtesasi, M.; Jamali, J. Quantitative assessment of desertification in south of Iran using MEDALUS method. *Environ. Monit. Assess.* **2007**, *134*, 243–254. [CrossRef]
31. Uzuner, Ç.; Dengiz, O. Desertification risk assessment in Turkey based on environmentally sensitive areas. *Ecol. Indic.* **2020**, *114*, 106295. [CrossRef]
32. Shao, W.; Wang, Q.; Guan, Q.; Zhang, J.; Yang, X.; Liu, Z. Environmental sensitivity assessment of land desertification in the Hexi Corridor, China. *Catena* **2023**, *220*, 106728. [CrossRef]
33. Ferrara, A.; Kosmas, C.; Salvati, L.; Padula, A.; Mancino, G.; Nolè, A. Updating the MEDALUS-ESA framework for worldwide land degradation and desertification assessment. *Land Degrad. Dev.* **2020**, *31*, 1593–1607. [CrossRef]
34. Guo, Z.; Wei, W.; Shi, P.; Zhou, L.; Wang, X. Spatiotemporal changes of land desertification sensitivity in the arid region of Northwest China. *Acta Geogr. Sin.* **2020**, *75*, 1948–1965. [CrossRef]
35. Wilson, A.M.; Jetz, W. Remotely sensed high-resolution global cloud dynamics for predicting ecosystem and biodiversity distributions. *PLoS Biol.* **2016**, *14*, e1002415. [CrossRef] [PubMed]
36. C Vega, G.; Pertierra, L.R.; Olalla-Tárraga, M.Á. MERRAclim, a high-resolution global dataset of remotely sensed bioclimatic variables for ecological modelling. *Sci. Data* **2017**, *4*, 170078. [CrossRef] [PubMed]
37. Gorelick, N.; Hancher, M.; Dixon, M.; Ilyushchenko, S.; Thau, D.; Moore, R. Google Earth Engine: Planetary-scale geospatial analysis for everyone. *Remote Sens. Environ.* **2017**, *202*, 18–27. [CrossRef]
38. Kumar, L.; Mutanga, O. Google Earth Engine Applications Since Inception: Usage, Trends, and Potential. *Remote Sens.* **2018**, *10*, 1509. [CrossRef]
39. Amani, M.; Ghorbanian, A.; Ahmadi, S.A.; Kakooei, M.; Moghimi, A.; Mirmazloumi, S.M.; Moghaddam, S.H.A.; Mahdavi, S.; Ghahremanloo, M.; Parsian, S. Google earth engine cloud computing platform for remote sensing big data applications: A comprehensive review. *IEEE J. Sel. Top. Appl. Earth Obs. Remote Sens.* **2020**, *13*, 5326–5350. [CrossRef]
40. Jamali, A.A.; Kalkhajeh, R.G.; Randhir, T.O.; He, S. Modeling relationship between land surface temperature anomaly and environmental factors using GEE and Giovanni. *J. Environ. Manag.* **2022**, *302*, 113970. [CrossRef]
41. Elnashar, A.; Zeng, H.; Wu, B.; Gebremicael, T.G.; Marie, K. Assessment of environmentally sensitive areas to desertification in the Blue Nile Basin driven by the MEDALUS-GEE framework. *Sci. Total Environ.* **2022**, *815*, 152925. [CrossRef]
42. Chen, X.; Bao, A.; Wang, X.; Hang, Y. Ecological Effect Evaluation of Comprehensive Control Project in Tarim River Basin. *Bull. Chin. Acad. Sci.* **2017**, *32*, 20–28. [CrossRef]

43. Fu, A.; Li, W.; Chen, Y.; Wang, Y.; Hao, H.; Li, Y.; Sun, F.; Zhou, H.; Zhu, C.; Hao, X. The effects of ecological rehabilitation projects on the resilience of an extremely drought-prone desert riparian forest ecosystem in the Tarim River Basin, Xinjiang, China. *Sci. Rep.* **2021**, *11*, 18485. [CrossRef] [PubMed]
44. Yu, T.; Liu, P.; Zhang, Q.; Ren, Y.; Yao, J. Detecting Forest Degradation in the Three-North Forest Shelterbelt in China from Multi-Scale Satellite Images. *Remote Sens.* **2021**, *13*, 1131. [CrossRef]
45. Zhu, B.; Yu, X.; Qin, X.; Liu, Z.; Xiong, H. Formation and evolution of sandy deserts in Xinjiang:The palaeo-environmental evidences. *Acta Geogr. Sin.* **2013**, *68*, 661–679. [CrossRef]
46. Li, X.; Jiang, F.; Li, L.; Wang, G. Spatial and temporal variability of precipitation concentration index, concentration degree and concentration period in Xinjiang, China. *Int. J. Climatol.* **2011**, *31*, 1679–1693. [CrossRef]
47. Spinoni, J.; Vogt, J.; Naumann, G.; Carrao, H.; Barbosa, P. Towards identifying areas at climatological risk of desertification using the Köppen–Geiger classification and FAO aridity index. *Int. J. Climatol.* **2015**, *35*, 2210–2222. [CrossRef]
48. National Center for Atmospheric Research (NCAR). TerraClimate: Global, High-Resolution Gridded Temperature, Precipitation, and Other Water Balance Variables. Available online: https://climatedataguide.ucar.edu/climate-data/terraclimate-global-high-resolution-gridded-temperature-precipitation-and-other-water (accessed on 9 June 2022).
49. Wang, J.; Wang, Y.; Yan, C.; Qi, Y. 1:100,000 Desert (Sand) Distribution Dataset in China. National Tibetan Plateau/Third Pole Environment Data Center. Available online: https://data.tpdc.ac.cn/zh-hans/data/122c9ac2-53ee-4b9a-ae87-1a980b131c9b/ (accessed on 9 June 2022).
50. Abatzoglou, J.T.; Dobrowski, S.Z.; Parks, S.A.; Hegewisch, K.C. TerraClimate, a high-resolution global dataset of monthly climate and climatic water balance from 1958–2015. *Sci. Data* **2018**, *5*, 170191. [CrossRef]
51. National Aeronautics and Space Administration (NASA). General Accuracy Statement of Vegetation Indices (MOD13). Available online: https://modis-land.gsfc.nasa.gov/ValStatus.php?ProductID=MOD13 (accessed on 9 June 2022).
52. Yang, Y.; Xiao, P.; Feng, X.; Li, H. Accuracy assessment of seven global land cover datasets over China. *ISPRS J. Photogramm. Remote Sens.* **2017**, *125*, 156–173. [CrossRef]
53. Uuemaa, E.; Ahi, S.; Montibeller, B.; Muru, M.; Kmoch, A. Vertical accuracy of freely available global digital elevation models (ASTER, AW3D30, MERIT, TanDEM-X, SRTM, and NASADEM). *Remote Sens.* **2020**, *12*, 3482. [CrossRef]
54. OpenLandMap. OpenLandMap Soil Organic Carbon Content. Available online: https://zenodo.org/record/2536040#.ZC7gvnZBxPY (accessed on 9 June 2022).
55. OpenLandMap. OpenLandMap Soil Sand Content. Available online: https://zenodo.org/record/1476852#.ZC7hInZBxPY (accessed on 9 June 2022).
56. OpenLandMap. OpenLandMap Soil Clay Content. Available online: https://zenodo.org/record/2525663#.ZC7hkHZBxPY (accessed on 9 June 2022).
57. United States Geological Survey (USGS). MOD13A2.061 Terra Vegetation Indices 16-Day Global 1 km. Available online: https://lpdaac.usgs.gov/products/mod13a2v061/ (accessed on 9 June 2022).
58. United States Geological Survey (USGS). MCD12Q1.061 MODIS Land Cover Type Yearly Global 500 m. Available online: https://lpdaac.usgs.gov/products/mcd12q1v061/ (accessed on 9 June 2022).
59. United States Geological Survey (USGS). MOD11A2.061 Terra Land Surface Temperature and Emissivity 8-Day Global 1 km. Available online: https://lpdaac.usgs.gov/products/mod11a2v061/ (accessed on 9 June 2022).
60. National Aeronautics and Space Administration (NASA). NASADEM: NASA NASADEM Digital Elevation 30 m. Available online: https://lpdaac.usgs.gov/products/nasadem_hgtv001/ (accessed on 9 June 2022).
61. Chardon, J.P.; Adriaensen, F.; Matthysen, E. Incorporating landscape elements into a connectivity measure: A case study for the Speckled wood butterfly (*Pararge aegeria* L.). *Landsc. Ecol.* **2003**, *18*, 561–573. [CrossRef]
62. Vignieri, S.N. Streams over mountains: Influence of riparian connectivity on gene flow in the Pacific jumping mouse (*Zapus trinotatus*). *Mol. Ecol.* **2005**, *14*, 1925–1937. [CrossRef]
63. Murad, A. Planning and location of health care services in Jeddah City, Saudi Arabia: Discussion of the constructive use of geographical information systems. *Geospat. Health* **2018**, *13*, 322–329. [CrossRef] [PubMed]
64. Liu, X.; Pan, Y.; Zhu, X.; Li, S. Spatiotemporal variation of vegetation coverage in Qinling-Daba Mountains in relation to environmental factors. *J. Geogr. Sci.* **2015**, *26*, 45–58. [CrossRef]
65. Pandey, B.K.; Khare, D. Identification of trend in long term precipitation and reference evapotranspiration over Narmada river basin (India). *Glob. Planet. Chang.* **2018**, *161*, 172–182. [CrossRef]
66. Waked, A.; Sauvage, S.; Borbon, A.; Gauduin, J.; Pallares, C.; Vagnot, M.-P.; Léonardis, T.; Locoge, N. Multi-year levels and trends of non-methane hydrocarbon concentrations observed in ambient air in France. *Atmos. Environ.* **2016**, *141*, 263–275. [CrossRef]
67. Song, Y.; Wang, J.; Ge, Y.; Xu, C. An optimal parameters-based geographical detector model enhances geographic characteristics of explanatory variables for spatial heterogeneity analysis: Cases with different types of spatial data. *GIScience Remote Sens.* **2020**, *57*, 593–610. [CrossRef]
68. Wang, J.; Xu, C. Geodetector: Principle and prospective. *Acta Geogr. Sin.* **2017**, *72*, 116–134. [CrossRef]
69. Du, Z.; Xu, X.; Zhang, H.; Wu, Z.; Liu, Y. Geographical Detector-Based Identification of the Impact of Major Determinants on Aeolian Desertification Risk. *PLoS ONE* **2016**, *11*, e0151331. [CrossRef]
70. Liu, Y.; Yang, R. The Spatial Characteristics and Formation Mechanism of the County Urbanization in China. *Acta Geogr. Sin.* **2012**, *67*, 1011–1020. [CrossRef]

71. Ren, Y.; Deng, L.; Zuo, S.; Luo, Y.; Shao, G.; Wei, X.; Hua, L.; Yang, Y. Geographical modeling of spatial interaction between human activity and forest connectivity in an urban landscape of southeast China. *Landsc. Ecol.* **2014**, *29*, 1741–1758. [CrossRef]
72. Zhang, M.; Kafy, A.-A.; Ren, B.; Zhang, Y.; Tan, S.; Li, J. Application of the optimal parameter geographic detector model in the identification of influencing factors of ecological quality in Guangzhou, China. *Land* **2022**, *11*, 1303. [CrossRef]
73. Meng, X.; Gao, X.; Lei, J.; Li, S. Development of a multiscale discretization method for the geographical detector model. *Int. J. Geogr. Inf. Sci.* **2021**, *35*, 1650–1675. [CrossRef]
74. Meng, Z.; Dang, X.; Gao, Y.; Ren, X.; Ding, Y.; Wang, M. Interactive effects of wind speed, vegetation coverage and soil moisture in controlling wind erosion in a temperate desert steppe, Inner Mongolia of China. *J. Arid Land* **2018**, *10*, 534–547. [CrossRef]
75. Daly, C.; Conklin, D.R.; Unsworth, M.H. Local atmospheric decoupling in complex topography alters climate change impacts. *Int. J. Climatol.* **2010**, *30*, 1857–1864. [CrossRef]
76. Veron, S.R.; Paruelo, J.M. Desertification alters the response of vegetation to changes in precipitation. *J. Appl. Ecol.* **2010**, *47*, 1233–1241. [CrossRef]
77. Li, F.; Zhao, W.; Liu, H. Productivity responses of desert vegetation to precipitation patterns across a rainfall gradient. *J. Plant Res.* **2015**, *128*, 283–294. [CrossRef] [PubMed]
78. Daham, A.; Han, D.; Rico-Ramirez, M.; Marsh, A. Analysis of NVDI variability in response to precipitation and air temperature in different regions of Iraq, using MODIS vegetation indices. *Environ. Earth Sci.* **2018**, *77*, 1–24. [CrossRef]
79. Liu, C.; Yan, X.; Jiang, F. Desert vegetation responses to the temporal distribution patterns of precipitation across the northern Xinjiang, China. *Catena* **2021**, *206*, 105544. [CrossRef]
80. Wang, Y. Phenological observations of short-lived and short-lived-like plants in early spring in Xinjiang. *Arid Zone Res.* **1993**, *10*, 34–39. [CrossRef]
81. Shan, N.; Shi, Z.; Yang, X.; Zhang, X.; Guo, H.; Zhang, B.; Zhang, Z. Trends in potential evapotranspiration from 1960 to 2013 for a desertification-prone region of China. *Int. J. Climatol.* **2016**, *36*, 3434–3445. [CrossRef]
82. Joseph, O.; Gbenga, A.E.; Langyit, D.G. Desertification risk analysis and assessment in Northern Nigeria. *Remote Sens. Appl. Soc. Environ.* **2018**, *11*, 70–82. [CrossRef]
83. Zhang, C.; Wang, X.; Li, J.; Hua, T. Identifying the effect of climate change on desertification in northern China via trend analysis of potential evapotranspiration and precipitation. *Ecol. Indic.* **2020**, *112*, 106141. [CrossRef]
84. Ziadat, F.M.; Taimeh, A.Y. Effect of rainfall intensity, slope, land use and antecedent soil moisture on soil erosion in an arid environment. *Land Degrad. Dev.* **2013**, *24*, 582–590. [CrossRef]
85. Xu, D.; You, X.; Xia, C. Assessing the spatial-temporal pattern and evolution of areas sensitive to land desertification in North China. *Ecol. Indic.* **2019**, *97*, 150–158. [CrossRef]
86. Karavitis, C.A.; Tsesmelis, D.E.; Oikonomou, P.D.; Kairis, O.; Kosmas, C.; Fassouli, V.; Ritsema, C.; Hessel, R.; Jetten, V.; Moustakas, N.; et al. A desertification risk assessment decision support tool (DRAST). *Catena* **2020**, 187. [CrossRef]
87. Curto, J.D.; Pinto, J.C. New multicollinearity indicators in linear regression models. *Int. Stat. Rev.* **2007**, *75*, 114–121. [CrossRef]
88. Ouyang, Z.; Wang, X.; Miao, H. China's eco-environmental sensitivity and its spatial heterogeneity. *Acta Ecol. Sin.* **1994**, *20*, 10–13. [CrossRef]
89. Zhao, M.; Zhao, W.; Jin, T.; An, Y.; Xu, H. Land Desertification Sensitivity Evaluation in Qinghai Lake Basin. *Chin. Agric. Sci. Bull.* **2012**, *28*, 32. [CrossRef]
90. Tian, L.; Qiu, S.; Peng, J.; Yina, H. Desertification sensitivity assessment in Inner Mongolia Autonomous Region based on PSR framework. *Prog. Geogr.* **2018**, *37*, 1682–1692. [CrossRef]
91. Zhang, F.; Yushanjiang, A.; Jing, Y. Assessing and predicting changes of the ecosystem service values based on land use/cover change in Ebinur Lake Wetland National Nature Reserve, Xinjiang, China. *Sci. Total Environ.* **2019**, *656*, 1133–1144. [CrossRef]
92. Jing, Y.; Zhang, F.; He, Y.; Johnson, V.C.; Arikena, M. Assessment of spatial and temporal variation of ecological environment quality in Ebinur Lake Wetland National Nature Reserve, Xinjiang, China. *Ecol. Indic.* **2020**, *110*, 105874. [CrossRef]
93. Ling, H.; Guo, B.; Zhang, G.; Xu, H.; Deng, X. Evaluation of the ecological protective effect of the "large basin" comprehensive management system in the Tarim River basin, China. *Sci. Total Environ.* **2019**, *650*, 1696–1706. [CrossRef] [PubMed]
94. Sun, B.; Wang, X. On Assessment of Sandy Desertification Sensitivity in Xinjiang. *J. Southwest China Norm. Univ. (Nat. Sci. Ed.)* **2015**, *40*, 108–112. [CrossRef]